remote sensing

MDPI

Article

Monitoring and Comparative Analysis of NO_2 and HCHO in Shanghai Using Dual-Azimuth Scanning MAX-DOAS and TROPOMI

Hongmei Ren [1], Ang Li [2,*], Zhaokun Hu [2], Nannan Shao [1], Xinyan Yang [1], Hairong Zhang [3], Jiangman Xu [2,4] and Jinji Ma [5]

[1] School of Physics and Electronic Information, Anhui Normal University, Wuhu 241000, China; hmren@ahnu.edu.cn (H.R.); 18255491703@163.com (N.S.); xinyanyang@ahnu.edu.cn (X.Y.)
[2] Key Laboratory of Environmental Optics and Technology, Anhui Institute of Optics and Fine Mechanics, Hefei Institutes of Physical Science, Chinese Academy of Sciences, Hefei 230031, China; zkhu@aiofm.ac.cn (Z.H.); jmxu@aiofm.ac.cn (J.X.)
[3] Cixi Branch of Ningbo Municipal Bureau of Ecology and Environment, Cixi 315302, China; hairong_z0903@163.com
[4] The Science Island Branch of Graduate School, University of Science and Technology of China, Hefei 230026, China
[5] School of Geography and Tourism, Anhui Normal University, Wuhu 241000, China; jinjima@mail.ahnu.edu.cn
* Correspondence: angli@aiofm.ac.cn

Abstract: This study employed dual-azimuth scanning MAX-DOAS to monitor vertical column densities of NO_2 and HCHO in Shanghai during the summer and winter of 2023, and compared the results with Sentinel-5P TROPOMI data. Dual-azimuth scanning revealed a generally consistent trend in gas concentrations ($r > 0.95$), but concentrations at 90° were higher than those at 0°, especially near the surface. This suggests that averaging multiple azimuth angles is necessary to better represent regional pollution levels. During the observation period, diurnal patterns revealed that NO_2 exhibited a "double peak" in the morning and evening, which was more pronounced in the summer, while HCHO peaked between 13:00 and 15:00. Comparisons with the TROPOMI data demonstrated overall good agreement. However, the probability of TROPOMI's NO_2 and HCHO measurements being lower than those of MAX-DOAS was 80% and 62.5%, respectively. Furthermore, TROPOMI tended to overestimate at high concentrations, with overestimation reaching 41.14% for NO_2 when exceeding 9.54×10^{15} molecules/cm^2 and 25.93% for HCHO when exceeding 1.26×10^{16} molecules/cm^2. Sensitivity analysis of the sampling distance (0–40 km) between TROPOMI samples and the ground-based site, and the sampling time (±5 to ±60 min) relative to the TROPOMI overpass, revealed that using a sampling distance of 15–25 km for NO_2 and 10–20 km for HCHO, along with appropriately shortening sampling times in the winter and extending them in the summer, can effectively enhance the consistency between satellite and ground-based observations. These findings not only reveal the spatiotemporal distribution characteristics of regional pollutants but optimize the sampling time and distance parameters for satellite–ground observation validation, providing data support for improving and enhancing the accuracy of satellite retrieval algorithms.

Keywords: nitrogen dioxide (NO_2); formaldehyde (HCHO); MAX-DOAS; TROPOMI; comparative analysis; Shanghai

check for updates

Academic Editor: Carmine Serio

Received: 17 December 2024
Revised: 12 January 2025
Accepted: 20 January 2025
Published: 22 January 2025

Citation: Ren, H.; Li, A.; Hu, Z.; Shao, N.; Yang, X.; Zhang, H.; Xu, J.; Ma, J. Monitoring and Comparative Analysis of NO_2 and HCHO in Shanghai Using Dual-Azimuth Scanning MAX-DOAS and TROPOMI. *Remote Sens.* **2025**, *17*, 355. https://doi.org/10.3390/rs17030355

Copyright: © 2025 by the authors. Licensee MDPI, Basel, Switzerland. This article is an open access article distributed under the terms and conditions of the Creative Commons Attribution (CC BY) license (https://creativecommons.org/licenses/by/4.0/).

1. Introduction

Ozone significantly impacts atmospheric chemistry, climate, and human health [1]. Stratospheric ozone shields the Earth from UV radiation, while tropospheric ozone is a major air pollutant, harmful to health and ecosystems [2]. Tropospheric ozone is mainly formed through photochemical reactions, in which nitrogen dioxide (NO_2) and formaldehyde (HCHO) act as essential precursors [3,4]. This process is particularly complex in urban and coastal regions where industrial activities, traffic emissions, and dense shipping contribute to elevated NO_2 and HCHO levels [5,6]. Consequently, ozone formation in these areas is influenced by multiple factors, such as human activity and marine meteorological conditions. Accurate monitoring of ozone precursors, like NO_2 and HCHO, can help identify sources of ozone pollution, elucidate its spatiotemporal distribution characteristics, and provide a scientific basis for air quality improvement.

Satellite remote sensing offers an efficient approach to monitoring concentrations of various air pollutants and particulate matter, including NO_2 and HCHO [7,8]. This technology enables broad geographic coverage, including remote regions and oceans, and supports long-term observation, which is essential for studying climate change and pollution trends. The European Space Agency's Sentinel-5 Precursor satellite, equipped with the Tropospheric Monitoring Instrument (TROPOMI), provides unprecedented accuracy and resolution for monitoring atmospheric components [9–11]. However, in practical applications, satellite remote sensing can be affected by atmospheric conditions, satellite orbits, and external interferences, potentially introducing some uncertainties in the data [12]. By contrast, ground-based observation technology can monitor atmospheric components, such as NO_2 and HCHO, in real-time through various methods, including fixed stations [13], drones [14], and marine vessels [15], providing more detailed and reliable data. To ensure data quality, ground-based observations are often used to validate the accuracy and reliability of satellite remote sensing data, thereby enhancing the overall effectiveness of atmospheric monitoring [16]. Thus, using ground-based observations to validate NO_2 and HCHO data from TROPOMI contributes to optimizing and improving the accuracy of satellite-based measurements.

Multi-Axis Differential Optical Absorption Spectroscopy (MAX-DOAS) is an advanced ground-based spectroscopic remote sensing technology that detects and quantifies atmospheric gas pollutants by observing scattered sunlight from various angles [17]. This technique not only provides high spatial resolution data on the vertical distribution of atmospheric components but offers unique advantages, such as flexible deployment, low cost, and the ability to simultaneously monitor multiple atmospheric constituents, including NO_2 and HCHO [18–21]. The accuracy of MAX-DOAS has been confirmed in many studies. For example, Zhang et al. compared the MAX-DOAS near-surface NO_2 data (50 m) in Shihezi City with data from a nearby monitoring station, with a correlation coefficient (R) of 0.75 [22]; Ren et al. compared the MAX-DOAS data in Shanghai with the European Centre for Medium-Range Weather Forecasts (ECMWF) CAMS model, obtaining correlation coefficients of 0.86 for NO_2 and 0.80 for HCHO [23]. These features make MAX-DOAS an ideal tool for validating the accuracy of NO_2 and HCHO data from the Sentinel-5P satellite. By comparing the TROPOMI data with ground-based measurements from MAX-DOAS, the reliability and accuracy of satellite remote sensing data can be effectively verified and calibrated.

Numerous studies have used ground-based MAX-DOAS to validate TROPOMI observations of NO_2 and HCHO over land and ocean regions, consistently finding strong agreement between satellite observations and ground-based measurements [24–28]. However, validation efforts for the Sentinel-5P satellite remain limited in complex coastal cities. In these regions, standard assumptions in satellite data processing—such as surface reflectance

uniformity and simplified atmospheric layering—may not hold, potentially impacting data accuracy. Therefore, validation and calibration of the satellite data in coastal urban settings are crucial. Shanghai, as China's economic hub and a major coastal metropolis, is an ideal location for environmental monitoring due to its high level of industrialization and dense population. Therefore, Shanghai's position at the land–sea interface provides an optimal environment for diversified satellite data validation, helping to assess the performance of Sentinel-5P under varied environmental conditions and improve data accuracy.

In summary, this study used ground-based dual-azimuth scanning MAX-DOAS remote sensing technology to measure the spatiotemporal distribution of NO_2 and HCHO vertical column concentrations in Shanghai during the summer and winter of 2023. These measurements were compared with the TROPOMI data from the same period to validate the accuracy of TROPOMI's NO_2 and HCHO observations in the complex land–sea interface environment. Additionally, this study explored and assessed the sensitivity of the validation results to two factors: sampling distance and sampling time.

2. Method and Instrument

2.1. MAX-DOAS Measurement

2.1.1. Site and Instrument

MAX-DOAS technology is based on passive differential optical absorption spectroscopy (DOAS) [17]. By adding multiple elevation angles by adjusting the telescope's direction on top of zenith observations, it captures solar scattered light to obtain the vertical distribution characteristics of atmospheric components, as shown in Figure 1.

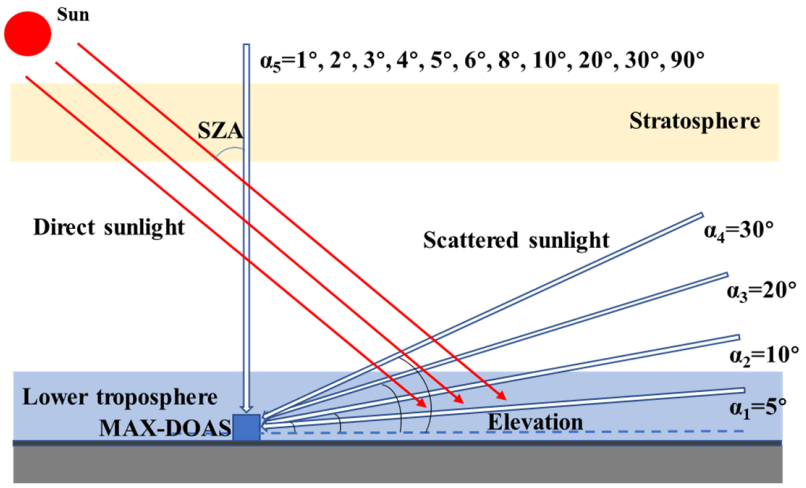


Figure 1. Schematic diagram of the MAX-DOAS measurement principle.

In this study, the MAX-DOAS instrument was installed at the Dongtan Comprehensive Atmospheric Observation Station on Chongming Island, Shanghai (31.60°N, 121.80°E). The station is located near the East China Sea at an elevation of 5 m, as shown in Figure 2a. Seasonal variations in atmospheric conditions, such as cloud cover and snow, can affect the accuracy of TROPOMI satellite observations. Therefore, this study was conducted during two periods: January and February of 2023 (representing winter) and May and June of 2023 (representing summer). Additionally, scanning in a single direction often fails to accurately reflect gas concentrations from other directions. To validate the accuracy of the Sentinel-5P satellite data, we employed scans at two azimuth angles to measure the tropospheric vertical column densities. Since the site offers unobstructed views to the due north (0°) and due east (90°), we set these two angles for alternate scanning, as depicted in Figure 2a. This observational method can improve the spatial colocation with Sentinel-5P measurements, thereby reducing the dispersion of the validation results.

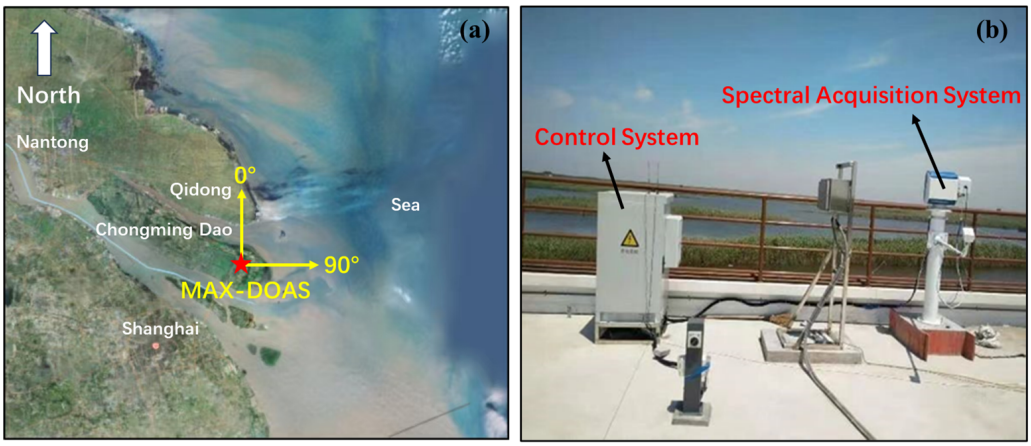


Figure 2. MAX-DOAS monitoring location (**a**) and equipment (**b**).

This study's MAX-DOAS instrument consists of two main modules: the spectroscopic acquisition system and the control system. The control system was housed within a moisture-proof, corrosion-resistant, and insulated cabinet, containing components such as power distribution, the spectrometer, a computer, and temperature control. The spectrometer, which is the core component of the equipment, is an Avantes model from the Netherlands with a wavelength range of 302–467 nm. The spectroscopic acquisition system primarily comprises a 360° rotating platform, a telescope, and a camera. The telescope was mounted on the rotating platform and controlled by a computer to collect spectra at various elevations and azimuth angles. The collected sunlight was scattered and then transmitted to the spectrometer via optical fiber for analysis. In this study, the telescope's field of view was approximately 0.1°, and it was set to scan at 11 different elevation angles (1°, 2°, 3°, 4°, 5°, 6°, 8°, 10°, 20°, 30°, and 90°) in each azimuth angle, with each cycle taking about 5 min. Within the same elevation angle measurement cycle, the differences in stratospheric absorption between elevation angles were negligible. Therefore, the spectrum at 90° from the same measurement cycle was used as the Fraunhofer reference spectrum (FRS) to eliminate strong Fraunhofer lines and stratospheric absorption. Elevation angles between 1° and 10° provide higher sensitivity to near-surface gas concentrations as they capture longer light paths through the boundary layer. Higher elevation angles (e.g., 20°, 30° and 90°) are primarily used for reference measurements and to reduce uncertainties in the retrieval process caused by atmospheric scattering and absorption. Below the platform, two surveillance cameras were installed to monitor the operational status of the equipment and weather conditions in real time. A photograph of the MAX-DOAS instrument is shown in Figure 2b.

2.1.2. Spectral Retrieval

The basic principle of retrieving gas concentrations using MAX-DOAS technology involves two steps: first, high-resolution spectrometers capture the solar scattered light spectra; then, these data are processed using DOAS retrieval to derive the differential slant column densities (DSCD) of target gases. Performing DOAS retrieval on the collected spectra is a crucial step in data processing. In this study, we used QDOAS version 3.2 (http://uv-vis.aeronomie.be/software/QDOAS/, accessed on 10 December 2024) for spectral evaluation. At the core of QDOAS is a least-squares algorithm that accurately analyzes observed spectra to precisely calculate the DSCDs of trace gases in the atmosphere. For NO_2 and HCHO, the spectral fitting windows were set to 338.2–370 nm and 336.5–359 nm, respectively. Figure 3 shows the spectral fitting results for NO_2 and HCHO observed at the MAX-DOAS site on Chongming Island, Shanghai, at 08:56:45 LT on 9 June 2023 (azimuth angle 90°, elevation angle 6°). Low elevation angles (e.g., 6°) typically balance a shorter light

path and a higher signal-to-noise ratio, effectively capturing the gas distribution characteristics in the near-surface layer. The NO_2 and HCHO DSCDs were 4.43×10^{16} molecules/cm^2 and 5.74×10^{16} molecules/cm^2, respectively, with root mean square (RMS) fitting errors of 7.85×10^{-4} and 8.80×10^{-4}, indicating a high-quality retrieval.

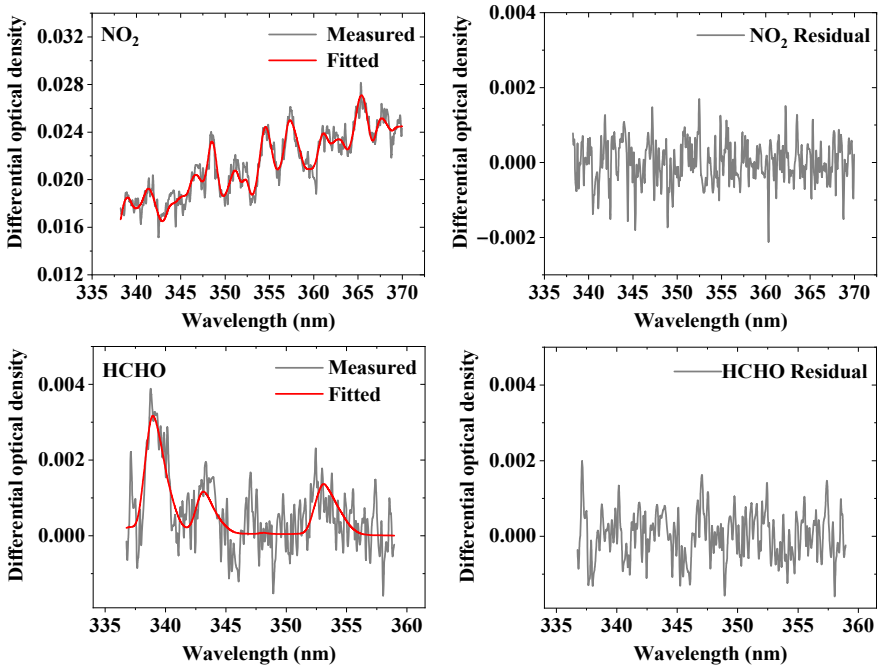


Figure 3. Schematic of NO_2 and HCHO retrieval (9 June 2023, 08:56:45 LT, azimuth angle 90°, elevation angle 6°).

To further derive the gas vertical column density (VCD) and profile, the measured differential gas DSCDs at different elevation angles, along with various atmospheric parameters must be input into an atmospheric radiative transfer model for calculation. The VCDs and vertical profiles are calculated from integrated measurements across all elevation angles (1°, 2°, 3°, etc.) at the specified azimuths (0° and 90°). In this study, the radiative transfer model used is SCIATRAN 2.2, and the profile retrieval algorithm is based on the PriAM method [19]. The retrieval parameter configuration for NO_2 and HCHO is based on the results of previous studies [23] and will not be elaborated upon here.

2.2. Sentinel-5P Satellite Data

The NO_2 VCD and HCHO VCD satellite data used in this study are sourced from Sentinel-5P's Level 2 data products, which are freely available from the European Space Agency's Sentinel Scientific Data Hub (https://dataspace.copernicus.eu, accessed on 12 December 2024). Launched by the European Space Agency in 2017, Sentinel-5P is a satellite dedicated to global atmospheric pollution monitoring. Its tropospheric monitoring instrument (TROPOMI) enables effective observation of various atmospheric trace gases worldwide, including NO_2, HCHO, SO_2, CH_4, CO, and aerosols [10]. TROPOMI is the first instrument under the European Union's Copernicus program specifically designed for high spatiotemporal resolution atmospheric measurements and is regarded as the most advanced and highest-resolution atmospheric monitoring spectrometer globally, covering ultraviolet, visible, near-infrared, and far-infrared wavelengths [29]. It provides daily global coverage, with a revisit frequency over the same geographical area once every day, which significantly enhances the temporal resolution of atmospheric observations. TROPOMI employs a top-down observation method, capturing backscattered sunlight from the Earth's surface and atmosphere. This observational approach provides a comprehensive view of

atmospheric trace gases, but it is relatively less sensitive to high concentrations of gases near the surface due to scattering effects and vertical column integration.

Since 2017, TROPOMI has achieved a spatial resolution of 7 km × 3.5 km, which was further enhanced to 3.5 km × 5.5 km on 6 August 2019 [30]. TROPOMI gas retrieval involves a processing module and a quality assurance module. The spectral retrieval process is similar to that of MAX-DOAS. First, radiometric and spectral corrections are performed, followed by georeferencing to accurately map observational data to ground locations. Next, the DOAS algorithm is applied to retrieve SCDs of NO_2 and HCHO from the measured reflectance spectra. TROPOMI's spectral fitting window for NO_2 differs slightly from that of MAX-DOAS in this study, covering the range of 405–465 nm. For HCHO, the fitting window is similar to that of MAX-DOAS, at 328.5–359 nm, a range that minimizes interference from other gases, such as ozone and BrO. The SCDs are converted into VCDs using air mass factors (AMFs), which account for light path geometries, cloud fraction, surface albedo, and a priori vertical profiles of the target gases. For weak absorbers, such as HCHO, additional steps, like background normalization, are applied to correct for biases and offsets in the retrieval process. Finally, data undergo quality control to generate standardized products. Since Shanghai is not always located at TROPOMI's nadir point, observations are affected by the viewing angle, resulting in a resolution slightly lower than the nadir resolution. The actual resolution is further influenced by factors, such as instrument calibration and data processing methods (e.g., interpolation), which can lead to variations in the final downloaded data resolution.

3. Results and Discussions

3.1. Comparison of Measurements from Two Azimuth Angles

The consistency of MAX-DOAS scanning results at different azimuth angles is influenced by time and geographic location. To assess the consistency of measurements at different azimuth angles (due north (0°) and due east (90°)) at the Shanghai Chongming Island site during the observation period, we conducted a detailed comparison of NO_2 and HCHO VCDs and profiles obtained from dual-azimuth scanning, as shown in Figures 4 and 5. Overall, both the winter and summer NO_2 and HCHO results show good trend consistency and high correlation across the two scanning angles. The Pearson correlation coefficients (r) for NO_2 VCD reached 0.964 in the winter and 0.954 in the summer (Figure 4b,d), while for HCHO VCD, they were 0.958 and 0.969, respectively (Figure 4f,h). Such high consistency facilitates the mutual validation of observational data from different angles in ground-based monitoring equipment. However, there was a slight difference between the observations from the two azimuth angles, with the 90° azimuth showing higher values than the 0° azimuth. Furthermore, Figure 4 indicates that NO_2 concentrations showed little seasonal variation between the winter and summer, while HCHO concentrations were significantly higher in the summer, with frequent high values, which was associated with the enhanced photochemical reactions in the summer [31].

Figure 5 shows the distribution of NO_2 and HCHO vertical profiles measured at azimuths of 0° and 90°. In this study, the PriAM algorithm outputs gas profile data within the altitude range of 0–4 km. MAX-DOAS operates as a bottom-up observation method, with its sensitivity to measuring NO_2 and HCHO generally concentrated at altitudes below 10 km. The detection sensitivity is higher below 4 km and gradually decreases with increasing altitude [32]. Additionally, the sensitivity range is influenced by atmospheric visibility: in cleaner weather conditions, the sensitivity range extends to higher altitudes, while in heavily polluted conditions, it may decrease. It is worth noting that the primary distribution of NO_2 and HCHO is concentrated near the surface. Specifically, NO_2 mainly originates from ground-level emissions (such as vehicle exhaust and industrial activities),

with concentrations typically distributed within the 0–2 km range [33]. HCHO, on the other hand, primarily results from the photochemical reactions of volatile organic compounds (VOCs) in the surface region, with concentrations typically concentrated within the 0–3 km range [31]. The concentrations of NO_2 and HCHO in the upper troposphere are extremely low. Therefore, MAX-DOAS can effectively capture the concentration variations of these gases in the troposphere.

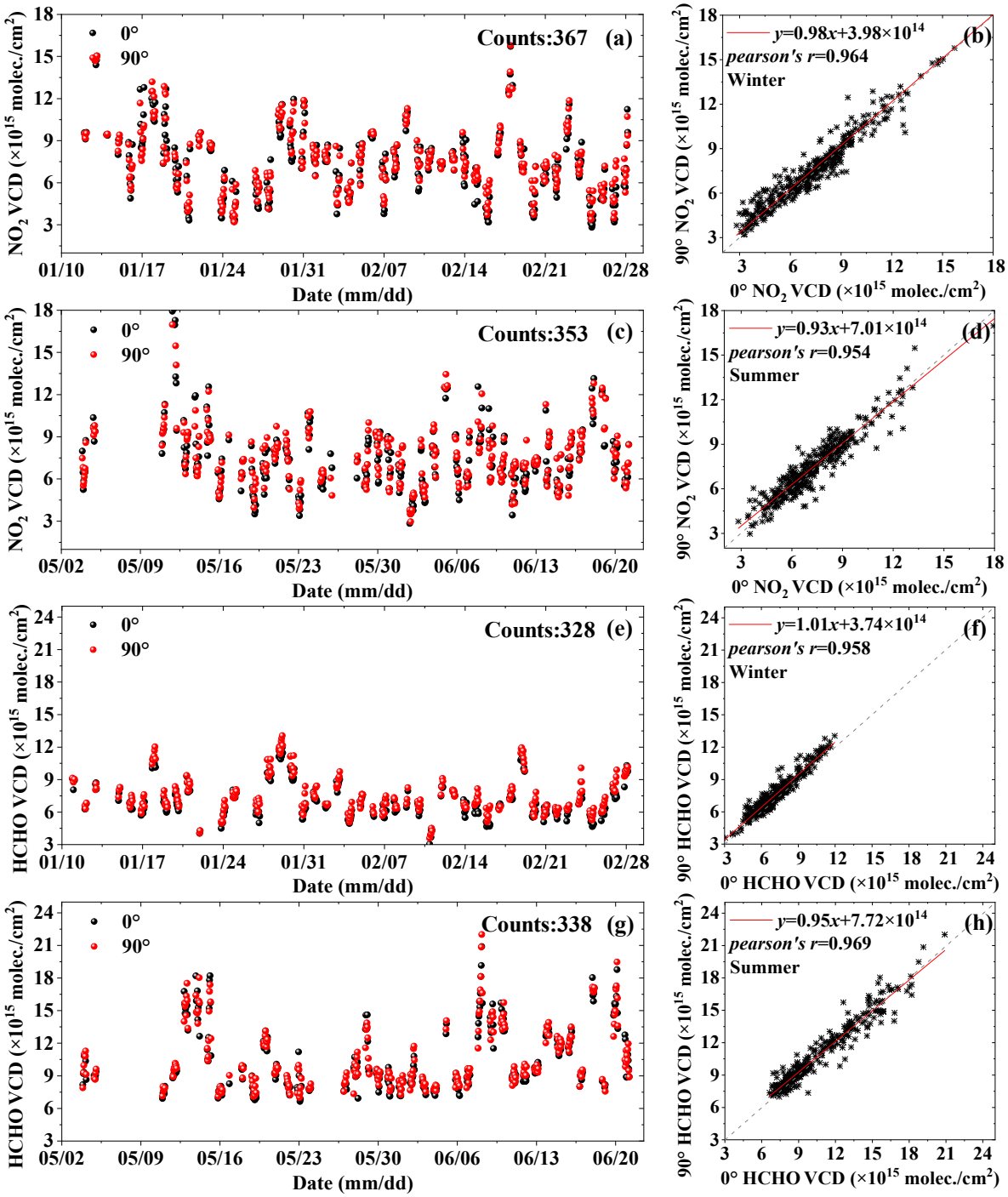


Figure 4. Comparison of NO_2 VCD (**a**–**d**) and HCHO VCD (**e**–**h**) measurements at 0° and 90° azimuth angles using the MAX-DOAS instrument.

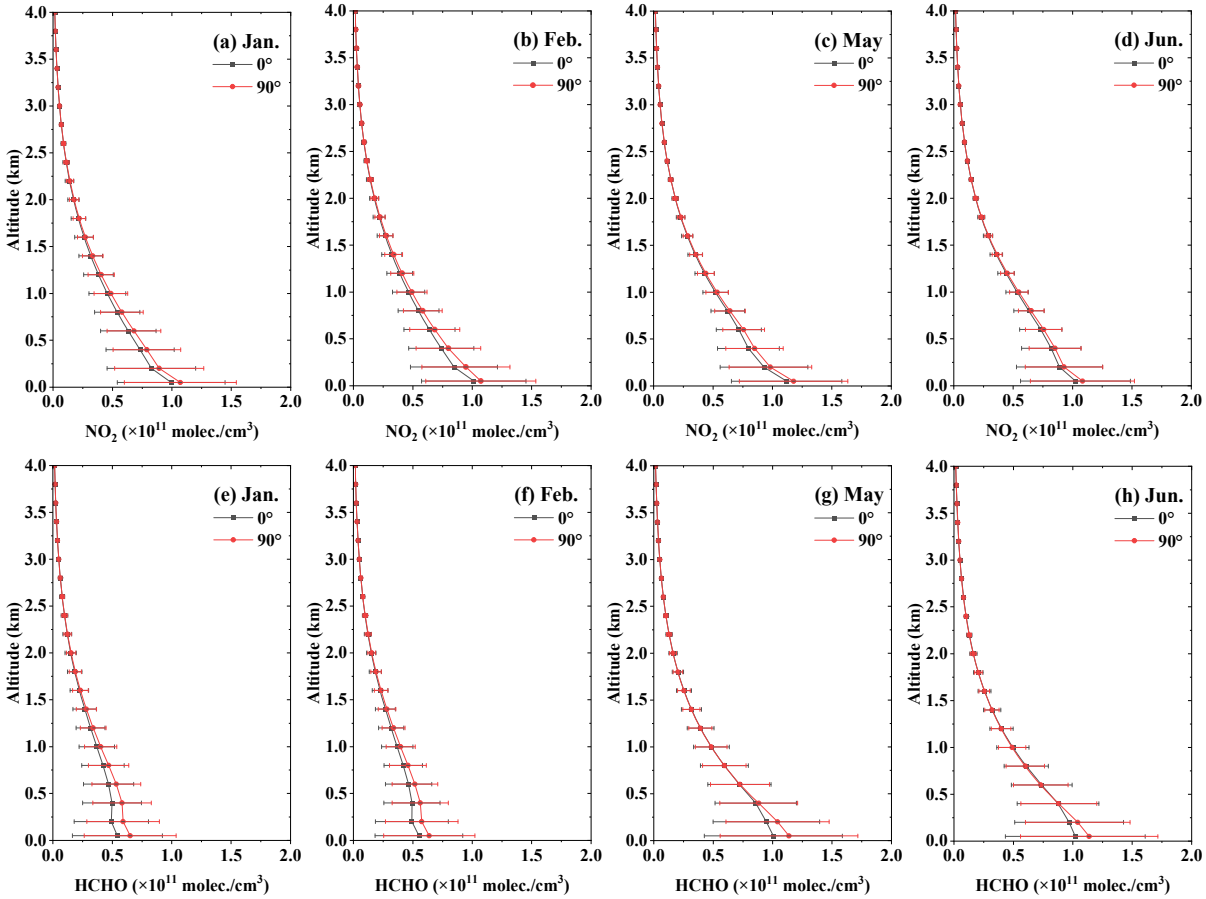


Figure 5. Comparison of NO_2 vertical profiles (**a**–**d**) and HCHO vertical profiles (**e**–**h**) measurements at 0° and 90° azimuth angles using the MAX-DOAS instrument.

The results of Figure 5 indicate that, at the Shanghai Chongming Island site, the distribution of NO_2 and HCHO in both azimuths exhibited a similar pattern across different months, following an exponential distribution with height, meaning the concentrations were highest near the ground. Similar to the VCD results, the concentrations at 90° were consistently higher than those at 0°, suggesting that pollutants were more likely to accumulate over the eastern marine area. Additionally, the difference in gas concentrations between the two angles is more pronounced at lower altitudes (below 1 km). This suggests that for MAX-DOAS, the average values from multiple azimuths will better reflect the pollutant distribution across the entire region compared to a single azimuth. However, monitoring from multiple azimuths requires specific environmental conditions at the site, including an unobstructed view in all directions. The southern direction is often avoided due to interference from direct sunlight. Considering the surrounding environmental factors at the Shanghai Chongming Island site, this study only utilizes observations from the 0° and 90° azimuths.

3.2. Diurnal and Weekly Variations of NO_2 and HCHO

Studies have shown that the concentrations of NO_2 and HCHO typically exhibit significant diurnal and weekly variations in industrialized areas and cities, closely related to anthropogenic emission sources, such as traffic and industrial activities [34]. For example, NO_2 often shows a "weekend effect" [35]. In this study, MAX-DOAS observation data were used to analyze the diurnal and weekly variations of tropospheric NO_2 VCD and HCHO VCD at the Shanghai Chongming Island site during both the winter and summer seasons, as shown in Figure 6. To more accurately represent the distribution of gas concentrations in

the surrounding area, the MAX-DOAS data used here were the averages from scans at two azimuth angles.

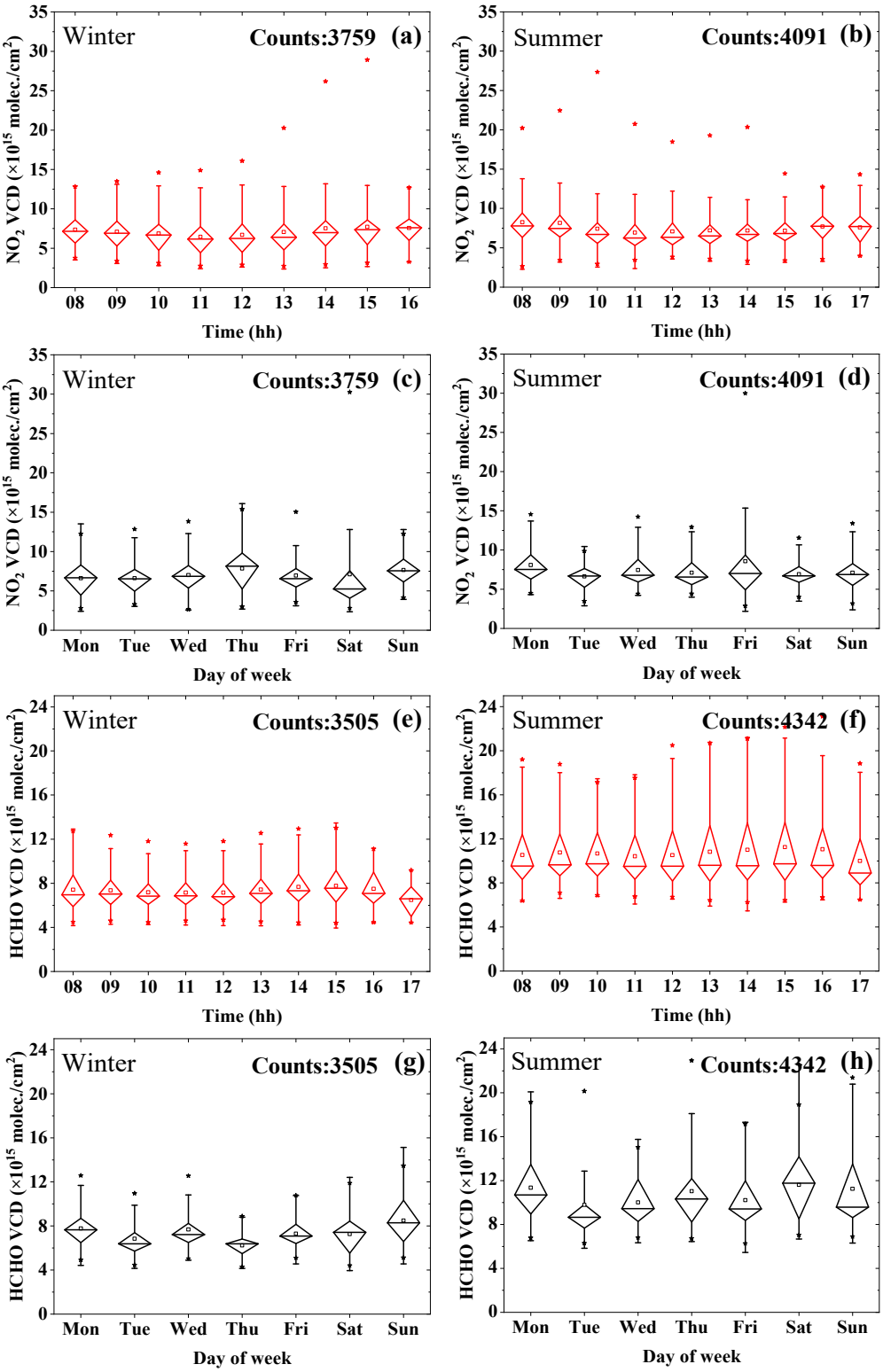


Figure 6. Diurnal (red) and weekly (black) variations of NO_2 and HCHO VCDs observed by MAX-DOAS: (**a**,**b**) diurnal variations of NO_2, (**c**,**d**) weekly variations of NO_2, (**e**,**f**) diurnal variations of HCHO, and (**g**,**h**) weekly variations of HCHO. The central black line in each box represents the median, and the hollow square in the center of each box indicates the mean value. The stars represent the 1% and 99% percentile values of the data.

Figure 6a–d shows the diurnal and weekly variations of NO_2 concentrations. The hourly average results indicate that NO_2 concentrations were higher in the morning and evening, with a decrease around noon, reaching the lowest value around 11:00, as shown in Figure 6a,b. This "bimodal" pattern is typically due to the increased traffic emissions during the morning and evening rush hours [36]. The "bimodal" feature of NO_2 was more pronounced in the summer (Figure 6b), which may be related to the enhanced photochemical consumption at noon during the summer months [37]. The weekly variation of NO_2 at the Shanghai Chongming Island site is shown in Figure 6c,d. The results indicate that there was no significant weekly trend in both the winter and summer. In the winter, the maximum mean NO_2 concentration occurred on Thursday at 7.84×10^{15} molecules/cm^2, while the minimum mean concentration was observed on Monday and Tuesday at 6.61×10^{15} molecules/cm^2. In the summer, the maximum mean NO_2 concentration was observed on Friday at 8.57×10^{15} molecules/cm^2, while the minimum mean concentration occurred on Tuesday at 6.63×10^{15} molecules/cm^2.

Figure 6e–h illustrate the diurnal and weekly variations in HCHO concentrations. The results showed that HCHO concentrations peaked between 13:00 and 15:00, as seen in Figure 6e,f. This indicates that the primary generation of HCHO occurs during the midday and afternoon periods, when the sunlight is strongest, which aligns with the active daytime period [38]. In the summer, the peak concentration of HCHO was significantly higher than in the winter, with a larger diurnal variation, which is likely associated with higher temperatures and stronger sunlight. The maximum hourly mean of HCHO in the summer reached 1.13×10^{16} molecules/cm^2, occurring at 15:00. The weekly variation of HCHO is shown in Figure 6g,h, with no typical "weekend effect" observed; instead, concentrations were higher during the weekend. In the winter, the highest mean concentration of HCHO occurred on Sunday, reaching 8.50×10^{15} molecules/cm^2, while in the summer, it peaked on Saturday at 1.16×10^{16} molecules/cm^2. Additionally, HCHO concentrations were higher on Mondays in both seasons. These patterns can be attributed to the main sources of HCHO, including increased biogenic emissions, active secondary photochemical reactions, meteorological conditions, and regional transport, all of which may contribute to elevated concentrations of HCHO [39]. This unconventional weekly variation further highlights the complexity of the HCHO formation.

3.3. Comparison Between MAX-DOAS and TROPOMI

Cross-validating remote sensing data from multiple platforms is essential for accurately assessing pollutant concentration changes. TROPOMI and MAX-DOAS have different spatial and temporal resolutions and, when using ground-based observations to validate and calibrate satellite data, variations in sampling space and time can directly impact the validation results. In this section, we compared NO_2 and HCHO observations from TROPOMI and MAX-DOAS and analyzed the sensitivity of the validation results to TROPOMI's sampling distance and MAX-DOAS's sampling time.

3.3.1. Time Series Comparison

Figure 7 shows the comparison of tropospheric NO_2 and HCHO concentration trends between TROPOMI and MAX-DOAS during the observation period, along with a correlation analysis. To ensure sufficient light intensity for spectral measurements in the winter, the observation time for MAX-DOAS was set from 08:00 to 17:00. The TROPOMI data we sampled represent the average concentration within a 10-km radius around the Shanghai Chongming Island site, while the MAX-DOAS data reflect the average concentration within $\pm$30 min of the satellite's overpass time. Additionally, we compared the results from

each azimuth angle (0° and 90°) as well as the averaged values from both angles with the TROPOMI data to evaluate their consistency.

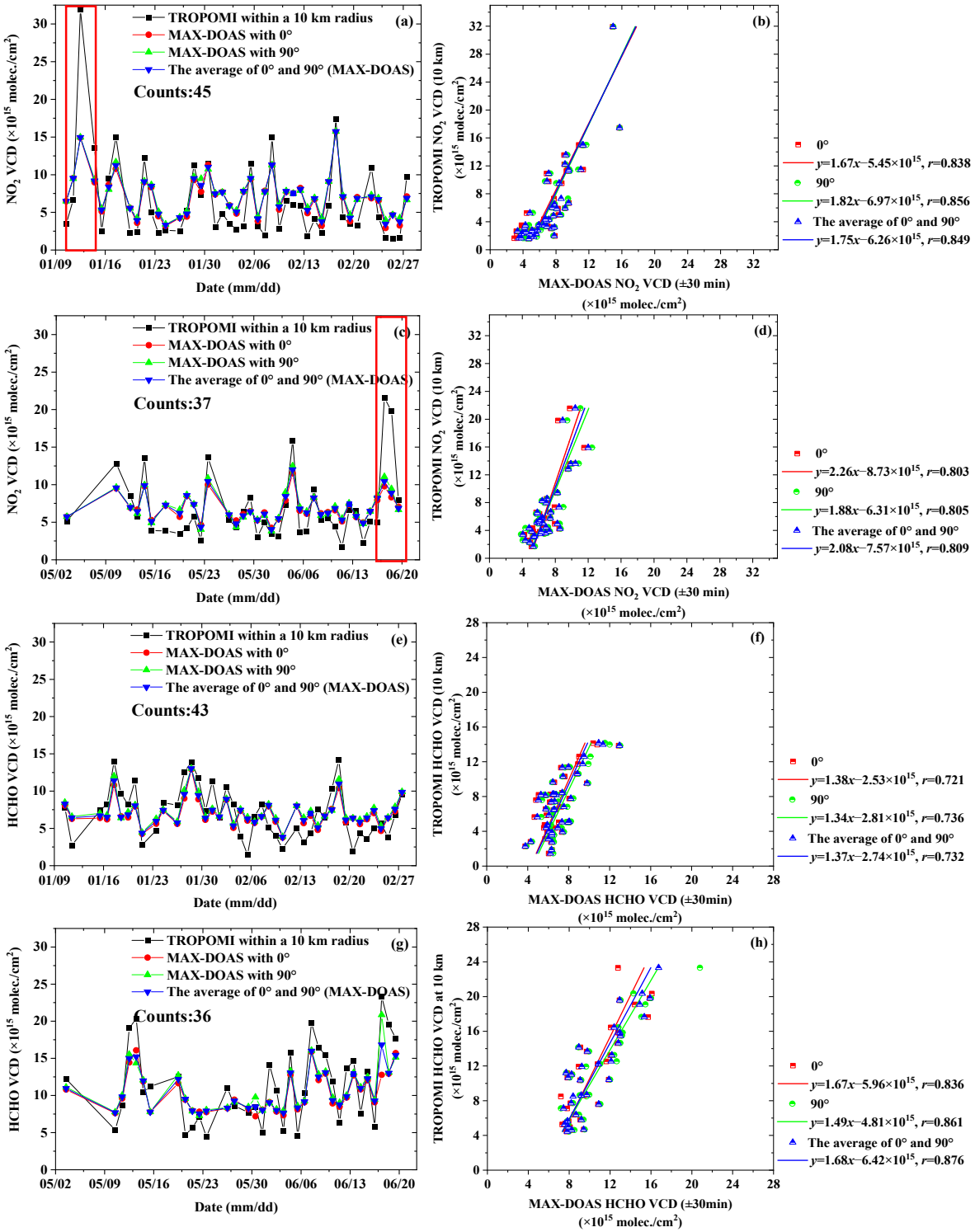


Figure 7. Variation trends and correlation analysis of tropospheric NO_2 and HCHO VCDs in Shanghai observed by TROPOMI and MAX-DOAS: (**a**,**c**) show NO_2 variation trends; (**e**,**g**) show HCHO variation trends; (**b**,**d**) show NO_2 correlation analysis; (**f**,**h**) show HCHO correlation analysis. The red boxes highlight the regions of high values.

The results indicated that both TROPOMI and MAX-DOAS observations of NO_2 and HCHO in the Shanghai area exhibited generally consistent temporal variation trends in both the winter and summer. However, the TROPOMI data tended to overestimate NO_2

and HCHO concentrations at higher levels and underestimate them at lower levels, as shown in Figure 7. This overestimation of NO_2 was particularly pronounced on 13 January, 18 June, and 19 June 2023, highlighted by the red boxes in Figure 7. This phenomenon aligned with findings from TROPOMI validation studies in other coastal cities, such as Helsinki and New York [40–42]. The differences between the two datasets may be related to the varying systematic errors introduced by the satellite and ground-based observation methods, as well as differences in the gas retrieval fitting windows.

The correlation analysis between the MAX-DOAS and TROPOMI data at the Shanghai Chongming Island site showed that the correlation coefficient for tropospheric NO_2 exceeded 0.80 (Figure 7b,d), indicating a good correlation, with NO_2 showing higher correlations in the winter than in the summer. For tropospheric HCHO, the correlation coefficient was significantly higher in the summer than in the winter (Figure 7f,h). In the winter, the correlation coefficients between TROPOMI and MAX-DOAS HCHO data for the 0°, 90°, and the average of both azimuth angles were 0.721, 0.736, and 0.732, respectively (Figure 7f). In the summer, these values increased to 0.836, 0.861, and 0.876 (Figure 7h), indicating better consistency between TROPOMI and MAX-DOAS under high HCHO concentration conditions. In the winter, the 90° azimuth angle data for NO_2 and HCHO showed the best agreement with TROPOMI, followed by the 0° data, with the average of both angles falling in between. In the summer, the average of the two azimuth angles shows the highest correlation with TROPOMI, with a correlation coefficient of 0.809 for NO_2 (Figure 7d) and 0.876 for HCHO (Figure 7h). Using the average of both angles expanded the spatial coverage of ground-based observations, allowing for better alignment with the TROPOMI data and reducing errors due to spatial discrepancies. Therefore, in the spatial and temporal sensitivity analyses in Sections 3.3.2 and 3.3.3, we used the averaged MAX-DOAS data from both azimuth angles. In terms of the regression slope, the slopes for NO_2 and HCHO exceeded 1 in both the winter and summer, indicating that TROPOMI observations generally overestimated the actual tropospheric concentrations of NO_2 and HCHO in the Shanghai area.

In inland areas, such as Beijing, the correlation coefficient between TROPOMI NO_2 data and MAX-DOAS exceeds 0.87 [20], while in oceanic regions, like the East China Sea, the correlation coefficient is also above 0.93 [24]. For HCHO, previous studies validated the TROPOMI data for Beijing from July 2018 to July 2019 using MAX-DOAS, finding a correlation coefficient above 0.80 [43]. According to our results, the correlation between TROPOMI-observed NO_2 and MAX-DOAS in Shanghai was noticeably lower than that in Beijing and the East China Sea, and the average correlation for HCHO across the winter and summer was also slightly lower than the results reported for Beijing. This suggests that TROPOMI's monitoring capacity may weaken in complex coastal terrains. Therefore, when validating satellite remote sensing data in such areas, it is essential to consider the influence of terrain and incorporate ground-based observations to adjust and calibrate the results, thereby improving accuracy.

3.3.2. Sampling Distance Sensitivity Analysis

In urban and industrial areas, due to dense traffic and industrial activities, the concentrations of NO_2 and HCHO may vary over scales of several hundred meters to several kilometers. The spatial sensitivity of MAX-DOAS can range from a few hundred meters to several tens of kilometers, depending on the environmental conditions, such as atmospheric transparency and scattering properties. We analyzed the correlation between the mean concentrations observed by TROPOMI within 0–40 km of the Shanghai ground-based site and the mean concentrations observed by MAX-DOAS within ±30 min of the satellite overpass time (see Supplementary Material Section S1). The horizontal axis represents

MAX-DOAS observations, while the vertical axis represents TROPOMI observations. For the comparison, the interval between observation pixels was set to 5 km.

Supplementary Materials, Figures S1 and S2 present the correlation analysis of NO_2 between satellite and ground-based observations at different sampling distances. The results showed that, when using only a single satellite pixel at the site location, the correlation coefficient with MAX-DOAS measurements was at its lowest, with values of 0.823 and 0.720 for the winter and summer, respectively. As the sampling distance increased, the correlation coefficient gradually rose, reaching its peak in the winter at 20 km and 25 km (r = 0.857 and r = 0.856, respectively), as shown in the Supplementary Materials, Figure S1. In the summer, the maximum correlation (r = 0.827) occurred at 15 km, with relatively high values also observed at 20 km and 25 km (r = 0.826), as shown in the Supplementary Materials, Figure S2. When the sampling distance extended beyond this range, the correlation coefficient slowly declined, dropping to 0.837 and 0.796 at 40 km for the winter and summer, respectively. The regression analysis reveals that the slopes of the regression lines exceeded 1 for both the winter and summer across different sampling distances, indicating that TROPOMI generally overestimated NO_2 VCD. Additionally, the regression slope in the winter was lower than in the summer, suggesting that TROPOMI's NO_2 observations were closer to MAX-DOAS measurements in the winter. The regression slope was highest when using only the site location and gradually decreased as the sampling distance increased. This pattern suggests that, as TROPOMI's sampling area appropriately expanded, the data may have smoothed out local high or low concentrations, making the values more comparable. Additionally, it is important to note that chemical reactions and atmospheric transport within this larger sampling area may further contribute to the observed differences between TROPOMI and MAX-DOAS measurements. Although a larger sampling distance brings the regression slope closer to 1, the correlation (or trend consistency) between the two datasets may have decreased. Overall, for coastal cities, like Shanghai, the optimal sampling distance for validating NO_2 data with satellite observations lies between 15 and 25 km; smaller or larger sampling ranges can reduce the consistency between ground-based and satellite observations.

Supplementary Materials, Figures S3 and S4 present the correlation analysis of HCHO between satellite and ground-based observations at different sampling distances. The results indicated that, at the site location (using only a single satellite pixel), there was no correlation between TROPOMI and MAX-DOAS HCHO measurements in the winter, while the correlation coefficient in the summer was 0.642. This suggests that a single satellite pixel cannot accurately reflect the HCHO concentrations observed by ground-based measurements. Therefore, when comparing satellite and ground-based observations, multiple satellite pixels over a certain range should be combined to better capture localized observational characteristics. As the sampling distance increased, the correlation coefficient for HCHO between satellite and ground-based data improved and showed some improvement. In the winter, it reached a maximum value (r = 0.796) at 15 km, as shown in the Supplementary Materials, Figure S3. In the summer, the highest correlation coefficients were observed between 10 km and 20 km, with the maximum at 10 km (r = 0.876). At 15 km and 20 km, the correlation coefficients were 0.866, as shown in the Supplementary Materials, Figure S4. As the sampling distance continued to increase, the correlation coefficient gradually decreased, similar to NO_2. At 40 km, the correlation coefficients dropped to 0.718 in the winter and 0.833 in the summer. The regression slopes corresponding to different sampling distances for HCHO were also similar to those for NO_2, with all values greater than 1. This indicates that TROPOMI also overestimated HCHO VCD overall. Unlike NO_2, the regression slope was lowest at the site location and increased as the sampling distance expanded, before slightly decreasing. Based on the correlation coefficient results, it can be concluded that, for

coastal cities like Shanghai, the optimal sampling distance for validating HCHO data with satellite observations lies between 10 and 20 km.

Figure 8 illustrates the variation in correlation coefficients and relative deviations of mean concentrations between TROPOMI and MAX-DOAS at different observation pixel distances. When the sampling distance between TROPOMI observation pixels and the ground-based site was too small, the correlation was low. As the sampling distance increased, the correlation gradually improved. A turning point in correlation was observed at approximately 15 km for NO_2 (Figure 8a) and at around 10 km for HCHO (Figure 8b). Beyond these distances, the correlation changed more slowly. The relative deviations for both NO_2 and HCHO were higher at the site location, particularly during the winter, at 41.37% and 62.54%, respectively, further indicating that the gas concentrations from a single pixel deviate significantly from ground-based observations [44]. With an appropriate increase in sampling distance, the relative deviation for NO_2 gradually decreased, eventually settling around 30%. For HCHO, the relative deviation first decreased and then stabilized beyond 10 km (at about 30%). These results suggest that, as the sampling distance increases, the probability of outliers in satellite observations reduces, meaning that averaging across multiple pixels allows satellite-observed NO_2 concentrations to better reflect regional pollution levels.

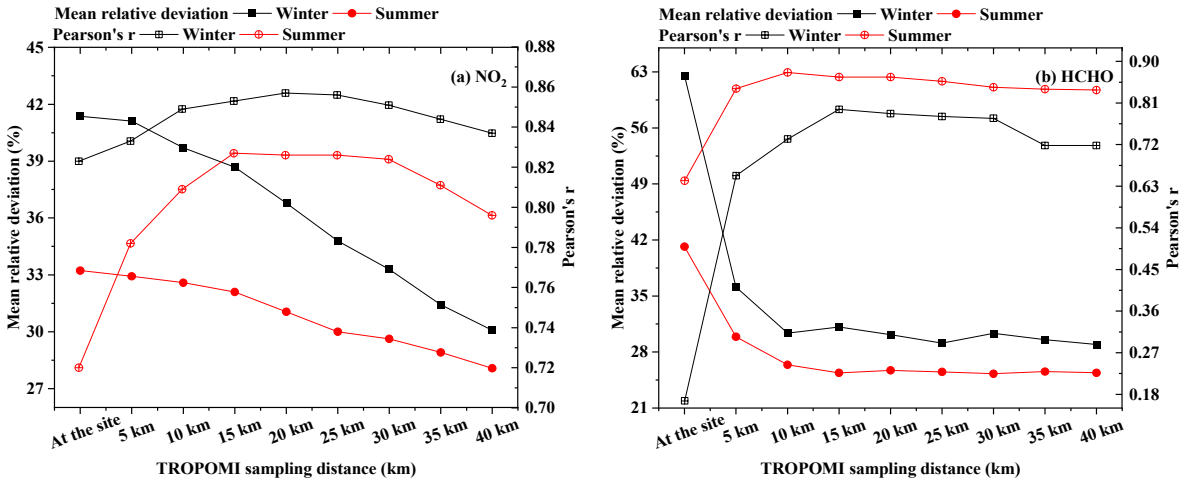


Figure 8. Correlation coefficients and relative deviations between the mean TROPOMI concentrations from observation pixels within 0–40 km of the Shanghai Chongming Island site and the mean MAX-DOAS concentrations within ±30 min of the satellite overpass: (**a**) NO_2; (**b**) HCHO.

3.3.3. Sampling Time Sensitivity Analysis

The concentrations of HCHO and NO_2 can vary significantly over time scales of minutes to hours, especially under specific environmental and meteorological conditions. These rapid changes are typically associated with factors such as traffic peaks, industrial activities, variations in solar radiation intensity, and local meteorological conditions (such as changes in wind speed and direction). Thus, the sampling time directly affects the consistency between satellite and ground-based comparisons. This section analyzes the sensitivity of sampling time. The scanning cycle for a single elevation angle with MAX-DOAS is approximately 5 min, while the cycle for the 0° and 90° azimuth angles takes about 10 min. Therefore, we selected the shortest sampling time range as ±5 min around the satellite overpass time. Additionally, due to factors, such as meteorological conditions and emission dynamics, excessively long sampling times can introduce significant errors. For example, aerosol loadings and the presence of interfering gases can significantly impact the sensitivity of the sampling parameters. The variability in aerosol optical properties and interfering gases may require longer averaging times to mitigate the short-term fluctuations

caused by these atmospheric components. This study chose a maximum time range of ±60 min. The correlation between the mean concentrations observed by satellite pixels within a 10 km radius of the ground-based site and the mean MAX-DOAS concentrations averaged over ±5 to ±60 min (a total sampling range of 10–120 min) from the TROPOMI overpass time was analyzed. The results are detailed in the Supplementary Materials, Section S2. The horizontal axis represents MAX-DOAS observations, while the vertical axis represents TROPOMI observations.

Supplementary Materials, Figures S5 and S6 show the correlation analysis of NO_2 observations between satellite and ground-based data at different sampling time ranges. In the winter (Supplementary Materials, Figure S5), the correlation coefficient remained relatively stable across different sampling time ranges, fluctuating slightly between 0.839 and 0.849. The highest correlation coefficient was observed at ±30 min (r = 0.849). Similarly, in the summer (Supplementary Materials, Figure S6), the correlation coefficient showed minimal variation, ranging from 0.786 to 0.819, with the highest value occurring at ±60 min (r = 0.819), followed by ±40 min (r = 0.813), with only a small difference between them. The regression slope gradually increased from ±5 min, reaching its maximum at ±30 min in the winter and ±40 min in the summer, before slightly decreasing over longer time ranges. Overall, the regression slope exhibited limited variation. The correlation analysis of HCHO observations was similar to that of NO_2, as shown in the Supplementary Materials, Figures S7 and S8. The correlation coefficient varied slightly across different time ranges, ranging from 0.723 to 0.749 in the winter and from 0.867 to 0.879 in the summer. The highest correlation coefficients were observed at ±10 min (r = 0.749) in the winter and ±60 min (r = 0.879) in the summer. The regression slope for HCHO also remained stable across different sampling time ranges. Additionally, the regression slopes for both NO_2 and HCHO were significantly lower in the winter than in the summer, indicating that TROPOMI and MAX-DOAS measurements were more closely aligned in the winter. The above results indicate that the sensitivity of the outcomes to sampling time was not as great as the sensitivity to sampling distance.

Overall, the correlation and regression slopes between satellite and ground-based observations for NO_2 and HCHO remained relatively stable with changes in sampling time. This indicates that different sampling intervals had a minimal impact on the agreement between the TROPOMI and MAX-DOAS data. It also suggests that NO_2 and HCHO concentrations around the observation site were relatively uniform, with localized fluctuations having a limited effect on the results. However, examining the correlation coefficients for the winter and summer reveals that the time intervals for achieving the highest correlation coefficients for NO_2 and HCHO in the winter (±30 min and ±10 min) were shorter than in the summer (±60 min for both). This implies that the instantaneous effects of local emission sources and meteorological conditions in the winter were more pronounced than in the summer. Consequently, when conducting validation comparisons between TROPOMI and MAX-DOAS, the averaging time for MAX-DOAS can be slightly shorter in winter and slightly longer in summer.

Figure 9 shows the variation in correlation coefficients and relative deviations of mean concentrations between TROPOMI and MAX-DOAS across different sampling times. The correlation coefficients remained relatively stable overall, with a notable increase for NO_2 in the summer at ±60 min (Figure 9a). The relative deviation results for NO_2 indicated that the shorter sampling times in the winter were associated with smaller deviations, while in the summer, smaller deviations were observed over longer sampling time ranges (Figure 9a). Overall, the relative deviations were greater in the winter than in the summer. This demonstrates the seasonal sensitivity of NO_2 to atmospheric conditions and emission dynamics. This suggests that, for NO_2 comparison and validation, the averaging time for

MAX-DOAS can be slightly shorter in winter and slightly longer in summer. For HCHO, the relative deviation varied more significantly with sampling time. Similar to NO_2, the overall relative deviations in the winter were greater than in the summer. In the winter, the deviation first increased and then decreased with sampling time; whereas, in the summer, it decreased steadily, stabilizing at around 25% (Figure 9b). This indicates that HCHO was more affected by localized fluctuations than NO_2. Extending the sampling time in the summer improves the consistency of HCHO results between satellite and ground-based observations. However, given that the satellite's overpass time over a city is typically only a few minutes, overly long averaging times may weaken the representativeness of the instantaneous satellite measurements. Conversely, since a single MAX-DOAS scan cycle takes approximately 5 min, overly short averaging times may introduce outliers into the data, reducing the validation effectiveness. Therefore, selecting a moderate sampling time window (±20–30 min in winter and ±30–40 min in summer) appears to be a more suitable balance for satellite–ground observation comparisons.

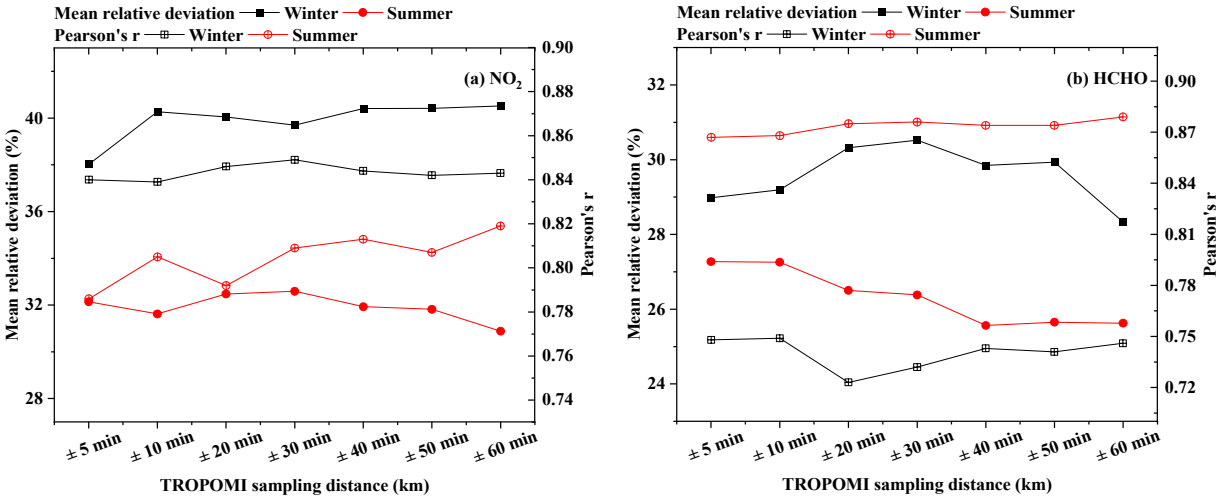


Figure 9. Correlation coefficients and relative deviations between the mean TROPOMI concentrations from observation pixels within 10 km of the Shanghai Chongming Island site and the mean MAX-DOAS concentrations averaged over ±5 to ±60 min of the satellite overpass: (**a**) NO_2; (**b**) HCHO.

To evaluate the performance of TROPOMI in observing NO_2 and HCHO at different concentration levels, we analyzed the variation in the deviations between the mean TROPOMI measurements within a 15 km spatial range and the mean MAX-DOAS measurements within a ±40-min time window as a function of concentration (Figure 10). To clearly illustrate the trend of these deviations, a polynomial fitting method was applied. The results indicated that the deviations for both NO_2 and HCHO increased with concentration, with NO_2 showing a more pronounced increase (Figure 10a). When the concentration exceeded a certain threshold, the deviations for both gases became positive, suggesting potential systematic overestimation or detection limit issues for TROPOMI in high-concentration regions. Conversely, at lower concentrations, many data points showed underestimation (deviations below zero). As shown in Figure 10, NO_2 was entirely overestimated when concentrations exceeded 9.54×10^{15} molecules/cm^2, while HCHO was entirely overestimated when concentrations exceeded 1.26×10^{16} molecules/cm^2. According to our statistical results, TROPOMI underestimated NO_2 concentrations by 22.66% when concentrations were below 9.54×10^{15} molecules/cm^2 but overestimated them by 41.14% when concentrations were above this threshold. For HCHO, TROPOMI underestimated concentrations by 12.16% below 1.26×10^{16} molecules/cm^2 and overestimated them by 25.93% above this threshold. Compared to the significant overestimation observed at high concentrations,

the probability of TROPOMI measurements being higher than those of MAX-DOAS was relatively low. Specifically, in this study, 80% of the TROPOMI NO_2 measurements were lower than those of MAX-DOAS, while 62.5% of the TROPOMI HCHO measurements were also lower than those of MAX-DOAS. Aerosol particles increase the scattering of light in the atmosphere, which can lead to a reduction in the intensity of light signals received by satellite sensors, especially in environments with high aerosol concentrations. This scattering effect may result in underestimations of the NO_2 and HCHO column densities observed from satellites, as the scattered light could "mask" the light absorption features of these gases.

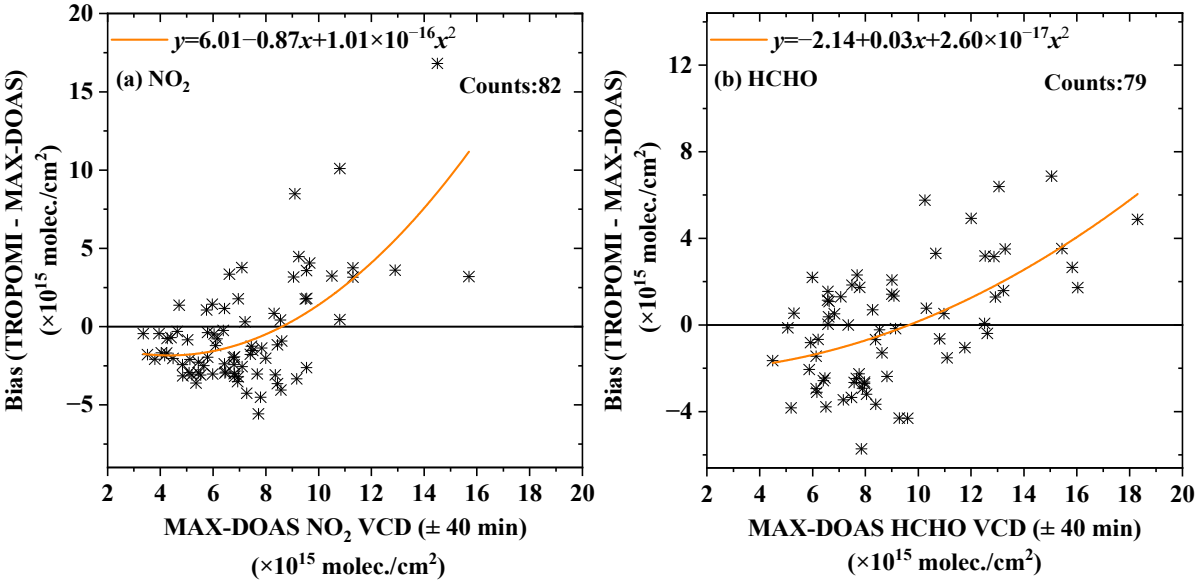


Figure 10. The variation in the deviations between the mean TROPOMI measurements within a 15 km spatial range and the mean MAX-DOAS measurements within a ±40-min time window as a function of concentration: (**a**) NO_2; (**b**) HCHO.

In summary, while TROPOMI was more likely to underestimate NO_2 and HCHO concentrations, the magnitude of overestimation was larger. These findings further highlight the need for improvement in TROPOMI algorithms, particularly in the retrieval of high-concentration values, for complex coastal urban terrains.

The above analysis discussed the sensitivity of sampling time and sampling distance, which is based on the assumption that measurements can represent a certain region within a fixed time. We also compared the MAX-DOAS concentrations nearest to the overpass time with the TROPOMI data from the pixel corresponding to the station location, as shown in Figure 11. The results indicate that the NO_2 measurements between MAX-DOAS and TROPOMI show good consistency, compared to the averages over larger temporal and spatial coverage. However, the correlation for HCHO was weaker in this case, with almost no correlation observed in the winter. This difference suggests that sampling time and spatial coverage are more critical for HCHO. Additionally, many days have missing TROPOMI values in the pixel corresponding to the MAX-DOAS site, resulting in a reduced number of valid comparisons.

These practical observations lead us to a broader discussion on the fundamental assumptions embedded in the retrieval algorithms for both MAX-DOAS and TROPOMI, which play a critical role in the interpretation and accuracy of the observed data. For instance, the plane-parallel atmosphere and single scattering approximations, while simplifying the computational models of MAX-DOAS retrievals, introduce limitations under certain atmospheric conditions, such as heavy aerosol loading or complex terrain. Similarly,

assumptions about cloud-free observations and uniform surface albedo in TROPOMI's retrieval process enhance data reliability under clear-sky conditions but may lead to inaccuracies when clouds are present. Understanding these assumptions is crucial for evaluating the sensitivity of the algorithms to varying atmospheric and surface conditions, thereby guiding improvements in data retrieval techniques and ensuring that the results are robust and applicable under diverse environmental settings.

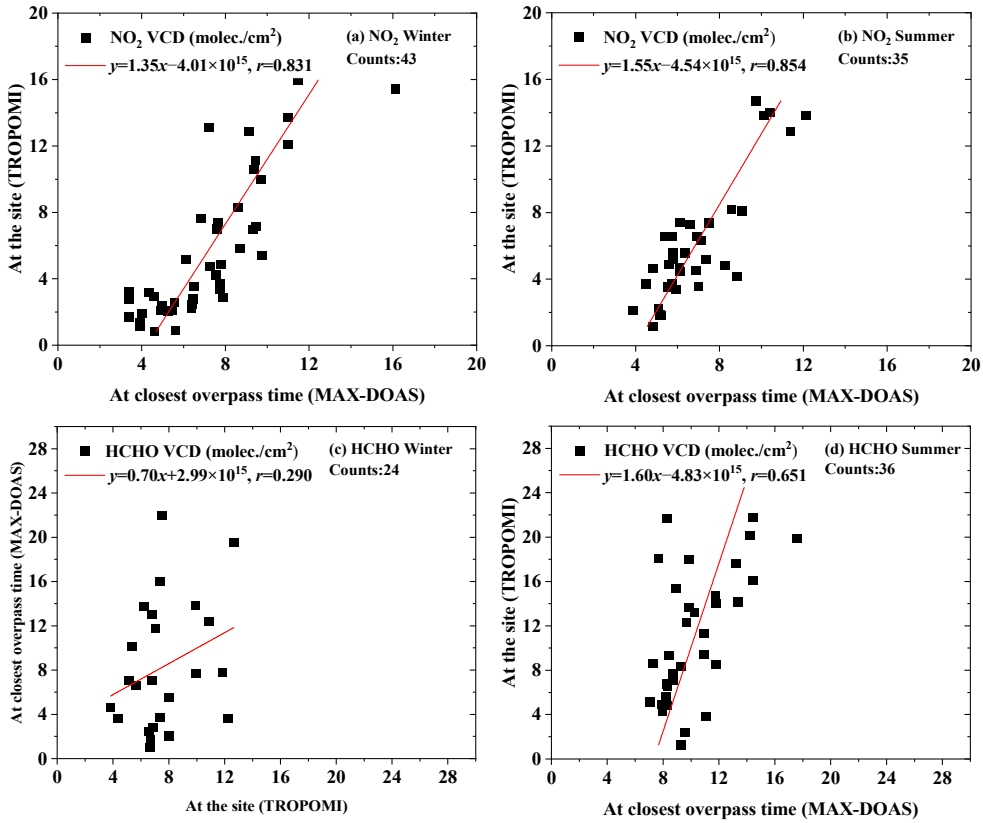


Figure 11. Comparison between MAX-DOAS measurements closest to the satellite overpass time and the corresponding TROPOMI data for the pixel containing the MAX-DOAS site.

4. Conclusions

In this study, collaborative observations from MAX-DOAS and TROPOMI were used to comprehensively analyze NO_2 and HCHO dynamics in the Shanghai area, focusing on variations across different azimuth angles (north and east) and seasons (summer and winter). The results showed that measurements from both azimuth angles exhibited generally consistent results (Pearson correlation coefficient, $r > 0.95$) in both the winter and summer. However, the concentration at the 90° azimuth was generally higher than that at 0°, especially near the surface. This indicates that, for MAX-DOAS, using the mean values from multiple azimuths provides a better representation of the pollution levels in a region. For diurnal variations, NO_2 displayed a "double peak" pattern in the morning and evening during both the winter and summer, while HCHO concentrations peaked mainly during the active photochemical reaction period in the afternoon. Additionally, HCHO concentrations were significantly higher in the summer than in the winter, closely linked to enhanced photochemical reactions under higher temperatures and stronger sunlight.

This study analyzed the consistency between NO_2 and HCHO data observed by TROPOMI and MAX-DOAS and investigated the impact of sampling distance and sampling time on satellite–ground data consistency. The results indicated that TROPOMI and MAX-DOAS measurements were generally consistent in most cases. However, TROPOMI

exhibited significant overestimation at high concentrations, particularly when NO_2 concentrations exceeded 9.54×10^{15} molecules/cm^2 and HCHO concentrations exceeded 1.26×10^{16} molecules/cm^2, with overestimation rates of 41.14% and 25.93%, respectively. Compared to overestimation, TROPOMI had a higher probability of reporting lower values than MAX-DOAS across all measurements. Statistical analysis of the experimental data showed that the probabilities of TROPOMI measurements being lower than MAX-DOAS for NO_2 and HCHO were 80% and 62.5%, respectively. These findings highlight that, while TROPOMI measurements overall demonstrate good consistency with MAX-DOAS, its performance across different concentration ranges requires further optimization, especially for high-concentration regions.

The sensitivity analysis of sampling distance indicated that correlation coefficients (r) between satellite and ground-based data increased initially and then declined as the sampling distance extended (0–40 km). Sampling distances of 15–25 km for NO_2 and 10–20 km for HCHO yielded the best match, suggesting that moderate sampling distances help mitigate the influence of localized high or low concentrations. Although the impact of sampling time on data consistency was smaller than that of sampling distance, shortening sampling times in the winter and extending them in the summer further improved consistency. Considering the instantaneous representativeness of satellite overpasses, choosing moderate sampling time windows ($\pm$20–30 min in winter, $\pm$30–40 min in summer) appears to be a more balanced approach.

In summary, this study not only revealed the spatiotemporal evolution of NO_2 and HCHO, key ozone precursors in Shanghai, but validated the TROPOMI satellite data using MAX-DOAS measurements, identifying the optimal sampling distances and times for ground-based validation in this region. These findings enhance our understanding of urban pollutant dynamics and provide critical support for improving the application of satellite remote sensing in coastal urban environmental monitoring.

Supplementary Materials: The following supporting information can be downloaded at: https://www.mdpi.com/article/10.3390/rs17030355/s1.

Author Contributions: Conceptualization, H.R. and A.L.; data curation, A.L. and Z.H.; formal analysis, H.R., N.S. and H.Z.; investigation, N.S., X.Y., H.Z. and J.X.; methodology, H.R.; project administration, H.R., A.L. and Z.H.; resources, A.L., Z.H., J.X. and J.M.; software, A.L. and Z.H.; supervision, A.L., X.Y. and J.M.; validation, H.R., N.S., X.Y. and H.Z.; visualization, N.S.; writing—original draft, H.R.; writing—review and editing, A.L., Z.H. and J.M. All authors have read and agreed to the published version of the manuscript.

Funding: This work was supported by the National Natural Science Foundation of China (No.: 42405135), the National Key Research and Development Project of China (No.: 2022YFC3703502, 2018YFC0213201), and the Local Service Project of Hefei (No.: 2020BFFFD01804).

Data Availability Statement: After the article is accepted, we are happy to share the data. Currently, the data are available upon request by email to Hongmei Ren at hmren@ahnu.edu.cn.

Acknowledgments: We acknowledge the European Space Agency (ESA) and the Copernicus program for providing free access to Sentinel-5P TROPOMI data, which played a crucial role in this study. We also thank the Belgian Institute for Space Aeronomy (BIRAIASB), Brussels, Belgium, for their freely accessible QDOAS software.

Conflicts of Interest: The authors declare no conflicts of interest.

References

1. Nuvolone, D.; Petri, D.; Voller, F. The effects of ozone on human health. *Environ. Sci. Pollut. Res.* **2018**, *25*, 8074–8088. [CrossRef] [PubMed]
2. Lefohn, A.S.; Malley, C.S.; Smith, L.; Wells, B.; Hazucha, M.; Simon, H.; Naik, V.; Mills, G.; Schultz, M.G.; Paoletti, E. Tropospheric ozone assessment report: Global ozone metrics for climate change, human health, and crop/ecosystem research. *Elem. Sci. Anthr.* **2018**, *6*, 28. [CrossRef] [PubMed]
3. Monks, P.S.; Archibald, A.; Colette, A.; Cooper, O.; Coyle, M.; Derwent, R.; Fowler, D.; Granier, C.; Law, K.S.; Mills, G. Tropospheric ozone and its precursors from the urban to the global scale from air quality to short-lived climate forcer. *Atmos. Chem. Phys.* **2015**, *15*, 8889–8973. [CrossRef]
4. Calvert, J.G.; Orlando, J.J.; Stockwell, W.R.; Wallington, T.J. *The Mechanisms of Reactions Influencing Atmospheric Ozone*; Oxford University Press: Oxford, UK, 2015.
5. Li, Y.; Wu, Z.; Ji, Y.; Chen, T.; Li, H.; Gao, R.; Xue, L.; Wang, Y.; Zhao, Y.; Yang, X. Comparison of the ozone formation mechanisms and VOCs apportionment in different ozone pollution episodes in urban Beijing in 2019 and 2020: Insights for ozone pollution control strategies. *Sci. Total Environ.* **2024**, *908*, 168332. [CrossRef]
6. Li, X.; Xie, P.; Li, A.; Xu, J.; Hu, Z.; Ren, H.; Zhong, H.; Ren, B.; Tian, X.; Huang, Y. Variation characteristics and transportation of aerosol, NO_2, SO_2, and HCHO in coastal cities of eastern China: Dalian, Qingdao, and Shanghai. *Remote Sens. Environ.* **2021**, *13*, 892. [CrossRef]
7. Johnson, M.S.; Souri, A.H.; Philip, S.; Kumar, R.; Naeger, A.; Geddes, J.; Judd, L.; Janz, S.; Sullivan, J. Satellite remote-sensing capability to assess tropospheric-column ratios of formaldehyde and nitrogen dioxide: Case study during the Long Island Sound Tropospheric Ozone Study 2018 (LISTOS 2018) field campaign. *Atmos. Meas. Tech.* **2023**, *16*, 2431–2454. [CrossRef]
8. AbdelSattar, A. Monitoring air pollution using satellite data. In Proceedings of the International Conference on Industrial Engineering and Operations Management, Toronto, ON, Canada, 23–25 October 2019; pp. 772–780.
9. Zhou, M.; Ni, Q.; Cai, Z.; Langerock, B.; Jiang, J.; Che, K.; Wang, J.; Nan, W.; Liu, Y.; Wang, P. Ground-Based Atmospheric CO_2, CH_4, and CO Column Measurements at Golmud in the Qinghai-Tibetan Plateau and Comparisons with TROPOMI/S5P Satellite Observations. *Adv. Atmos. Sci.* **2023**, *40*, 223–234. [CrossRef]
10. Levelt, P.F.; Stein Zweers, D.C.; Aben, I.; Bauwens, M.; Borsdorff, T.; De Smedt, I.; Eskes, H.J.; Lerot, C.; Loyola, D.G.; Romahn, F. Air quality impacts of COVID-19 lockdown measures detected from space using high spatial resolution observations of multiple trace gases from Sentinel-5P/TROPOMI. *Atmos. Chem. Phys.* **2021**, *22*, 10319–10351. [CrossRef]
11. Fioletov, V.; McLinden, C.A.; Griffin, D.; Theys, N.; Loyola, D.G.; Hedelt, P.; Krotkov, N.A.; Li, C. Anthropogenic and volcanic point source SO_2 emissions derived from TROPOMI on board Sentinel-5 Precursor: First results. *Atmos. Chem. Phys.* **2020**, *20*, 5591–5607. [CrossRef]
12. Wen, J.; Wu, X.; You, D.; Ma, X.; Ma, D.; Wang, J.; Xiao, Q. The main inherent uncertainty sources in trend estimation based on satellite remote sensing data. *Theor. Appl. Climatol.* **2023**, *151*, 915–934. [CrossRef]
13. Ren, B.; Xie, P.; Xu, J.; Li, A.; Qin, M.; Hu, R.; Zhang, T.; Fan, G.; Tian, X.; Zhu, W. Vertical characteristics of NO_2 and HCHO, and the ozone formation regimes in Hefei, China. *Sci. Total Environ.* **2022**, *823*, 153425. [CrossRef] [PubMed]
14. Rohi, G.; Ofualagba, G. Autonomous monitoring, analysis, and countering of air pollution using environmental drones. *Heliyon* **2020**, *6*, e03252. [CrossRef] [PubMed]
15. Tan, W.; Liu, C.; Wang, S.; Xing, C.; Su, W.; Zhang, C.; Xia, C.; Liu, H.; Cai, Z.; Liu, J. Tropospheric NO_2, SO_2, and HCHO over the East China Sea, using ship-based MAX-DOAS observations and comparison with OMI and OMPS satellite data. *Atmos. Chem. Phys.* **2018**, *18*, 15387–15402. [CrossRef]
16. Jafari, S.M.; Nikoo, M.R.; Dehghani, M.; Alijanian, M. Evaluation of two satellite-based products against ground-based observation for drought analysis in the southern part of Iran. *Nat. Hazards* **2020**, *102*, 1249–1267. [CrossRef]
17. Hönninger, G.; Von Friedeburg, C.; Platt, U. Multi axis differential optical absorption spectroscopy (MAX-DOAS). *Atmos. Chem. Phys.* **2004**, *4*, 231–254. [CrossRef]
18. Ji, X.; Liu, C.; Wang, Y.; Hu, Q.; Lin, H.; Zhao, F.; Xing, C.; Tang, G.; Zhang, J.; Wagner, T. Ozone profiles without blind area retrieved from MAX-DOAS measurements and comprehensive validation with multi-platform observations. *Remote Sens. Environ.* **2023**, *284*, 113339. [CrossRef]
19. Wang, Y.; Dörner, S.; Donner, S.; Böhnke, S.; De Smedt, I.; Dickerson, R.R.; Dong, Z.; He, H.; Li, Z.; Li, Z. Vertical profiles of NO_2, SO_2, HONO, HCHO, CHOCHO and aerosols derived from MAX-DOAS measurements at a rural site in the central western North China Plain and their relation to emission sources and effects of regional transport. *Atmos. Chem. Phys.* **2019**, *19*, 5417–5449. [CrossRef]

20. Kang, Y.; Tang, G.; Li, Q.; Liu, B.; Cao, J.; Hu, Q.; Wang, Y. Evaluation and evolution of MAX-DOAS-observed vertical NO_2 profiles in urban Beijing. *Adv. Atmos. Sci.* **2021**, *38*, 1188–1196. [CrossRef]
21. Tian, X.; Chen, M.; Xie, P.; Xu, J.; Li, A.; Ren, B.; Zhang, T.; Fan, G.; Wang, Z.; Zheng, J. Evaluation of MAX-DOAS Profile Retrievals under Different Vertical Resolutions of Aerosol and NO_2 Profiles and Elevation Angles. *Remote Sens.* **2023**, *15*, 5431. [CrossRef]
22. Zhang, H.; Li, A.; Wang, S.; Qin, M.; Hu, Z.; Xu, J. O_3 sensitivity and vertical distribution of summertime HCHO, NO_2, and SO_2 in Shihezi, China. *Atmos. Pollut. Res.* **2024**, *15*, 102113. [CrossRef]
23. Ren, H.; Li, A.; Hu, Z.; Zhang, H.; Xu, J.; Yang, X.; Ma, J.; Wang, S. MAX-DOAS observations of pollutant distribution and transboundary transport in typical regions of China. *J. Environ. Sci.* **2025**, *151*, 652–666. [CrossRef] [PubMed]
24. Wang, P.; Piters, A.; van Geffen, J.; Tuinder, O.; Stammes, P.; Kinne, S. Shipborne MAX-DOAS measurements for validation of TROPOMI NO_2 products. *Atmos. Meas. Tech.* **2020**, *13*, 1413–1426. [CrossRef]
25. Chan, K.L.; Geffen, J.V.; Smedt, I.D.; Alberti, C.; Cheng, Z.B. MAX-DOAS measurements of tropospheric NO_2 and HCHO in Munich and the comparison to OMI and TROPOMI satellite observations. *Atmos. Meas. Tech.* **2020**, *13*, 4499–4520. [CrossRef]
26. Iqbal, A.; Ahmad, N.; ud Din, H.M.; Van Roozendael, M.; Anjum, M.S.; Khan, M.Z.A.; Khokhar, M.F. Retrieval of NO2 Columns by Exploiting MAX-DOAS Observations and Comparison with OMI and TROPOMI Data during the Time Period of 2015–2019. *Aerosol Air Qual. Res.* **2022**, *22*, 210398. [CrossRef]
27. Rawat, P.; Naja, M.; Rajwar, M.C.; Irie, H.; Lerot, C.; Kumar, M.; Lal, S. Long-term observations of NO_2, SO_2, HCHO, and CHOCHO over the Himalayan foothills: Insights from MAX-DOAS, TROPOMI, and GOME-2. *Atmos. Environ.* **2024**, *336*, 120746. [CrossRef]
28. Yombo Phaka, R.; Merlaud, A.; Pinardi, G.; Friedrich, M.M.; Van Roozendael, M.; Müller, J.-F.; Stavrakou, T.; De Smedt, I.; Hendrick, F.; Dimitropoulou, E. Ground-based Multi-AXis Differential Optical Absorption Spectroscopy (MAX-DOAS) observations of NO_2 and H_2CO at Kinshasa and comparisons with TROPOMI observations. *Atmos. Meas. Tech.* **2023**, *16*, 5029–5050. [CrossRef]
29. Argyrouli, A.; Loyola, D.; Romahn, F.; Lutz, R.; Molina García, V.; Hedelt, P.; Heue, K.-P.; Siddans, R. An advanced spatial coregistration of cloud properties for the atmospheric Sentinel missions: Application to TROPOMI. *Atmos. Meas. Tech.* **2024**, *17*, 6345–6367. [CrossRef]
30. Van Geffen, J.; Boersma, K.F.; Eskes, H.; Sneep, M.; Ter Linden, M.; Zara, M.; Veefkind, J.P. S5P TROPOMI NO_2 slant column retrieval: Method, stability, uncertainties and comparisons with OMI. *Atmos. Meas. Tech.* **2020**, *13*, 1315–1335. [CrossRef]
31. Sun, Y.; Yin, H.; Liu, C.; Zhang, L.; Cheng, Y.; Palm, M.; Notholt, J.; Lu, X.; Vigouroux, C.; Zheng, B. Mapping the drivers of formaldehyde (HCHO) variability from 2015 to 2019 over eastern China: Insights from Fourier transform infrared observation and GEOS-Chem model simulation. *Atmos. Chem. Phys.* **2021**, *21*, 6365–6387. [CrossRef]
32. Kumar, V.; Beirle, S.; Dörner, S.; Mishra, A.K.; Donner, S.; Wang, Y.; Sinha, V.; Wagner, T. Long-term MAX-DOAS measurements of NO_2, HCHO, and aerosols and evaluation of corresponding satellite data products over Mohali in the Indo-Gangetic Plain. *Atmos. Chem. Phys.* **2020**, *20*, 14183–14235. [CrossRef]
33. Noxon, J.F. Tropospheric no2. *J. Geophys. Res. Oceans* **1978**, *83*, 3051–3057. [CrossRef]
34. Shao, M.; Zhang, Y.; Zeng, L.; Tang, X.; Zhang, J.; Zhong, L.; Wang, B. Ground-level ozone in the Pearl River Delta and the roles of VOC and NOx in its production. *J. Environ. Manag.* **2009**, *90*, 512–518. [CrossRef] [PubMed]
35. Beirle, S.; Platt, U.; Wenig, M.; Wagner, T. Weekly cycle of NO_2 by GOME measurements: A signature of anthropogenic sources. *Atmos. Chem. Phys.* **2003**, *3*, 2225–2232. [CrossRef]
36. Lähde, T.; Niemi, J.V.; Kousa, A.; Rönkkö, T.; Karjalainen, P.; Keskinen, J.; Frey, A.; Hillamo, R.; Pirjola, L. Mobile particle and NOx emission characterization at helsinki downtown: Comparison of different traffic flow areas. *Aerosol Air Qual. Res.* **2014**, *14*, 1372–1382. [CrossRef]
37. Zhang, Q.; Shen, Z.; Cao, J.; Zhang, R.; Zhang, L.; Huang, R.-J.; Zheng, C.; Wang, L.; Liu, S.; Xu, H. Variations in PM2. 5, TSP, BC, and trace gases (NO_2, SO_2, and O_3) between haze and non-haze episodes in winter over Xi'an, China. *Atmos. Environ.* **2015**, *112*, 64–71. [CrossRef]
38. Tian, X.; Xie, P.; Xu, J.; Li, A.; Wang, Y.; Qin, M.; Hu, Z. Long-term observations of tropospheric NO_2, SO_2 and HCHO by MAX-DOAS in Yangtze River Delta area, China. *J. Environ. Sci.* **2018**, *71*, 207–221. [CrossRef]
39. Liu, T.; Lin, Y.; Chen, J.; Chen, G.; Yang, C.; Xu, L.; Li, M.; Fan, X.; Zhang, F.; Hong, Y. Pollution mechanisms and photochemical effects of atmospheric HCHO in a coastal city of southeast China. *Sci. Total Environ.* **2023**, *859*, 160210. [CrossRef]
40. Ialongo, I.; Virta, H.; Eskes, H.; Hovila, J.; Douros, J. Comparison of TROPOMI/Sentinel-5 Precursor NO_2 observations with ground-based measurements in Helsinki. *Atmos. Meas. Tech.* **2020**, *13*, 205–218. [CrossRef]
41. Oomen, G.-M.; Müller, J.-F.; Stavrakou, T.; De Smedt, I.; Blumenstock, T.; Kivi, R.; Makarova, M.; Palm, M.; Röhling, A.; Té, Y. Weekly derived top-down volatile-organic-compound fluxes over Europe from TROPOMI HCHO data from 2018 to 2021. *Atmos. Chem. Phys.* **2024**, *24*, 449–474. [CrossRef]
42. Goldberg, D.L.; Tao, M.; Kerr, G.H.; Ma, S.; Tong, D.Q.; Fiore, A.M.; Dickens, A.F.; Adelman, Z.E.; Anenberg, S.C. Evaluating the spatial patterns of US urban NOx emissions using TROPOMI NO_2. *Remote Sens. Environ.* **2024**, *300*, 113917. [CrossRef]

43. Su, W.; Liu, C.; Chan, K.L.; Hu, Q.; Liu, H.; Ji, X.; Zhu, Y.; Liu, T.; Zhang, C.; Chen, Y. An improved TROPOMI tropospheric HCHO retrieval over China. *Atmos. Meas. Tech.* **2020**, *13*, 6271–6292. [CrossRef]
44. Dimitropoulou, E.; Hendrick, F.; Pinardi, G.; Friedrich, M.M.; Merlaud, A.; Tack, F.; De Longueville, H.; Fayt, C.; Hermans, C.; Laffineur, Q. Validation of TROPOMI tropospheric NO_2 columns using dual-scan multi-axis differential optical absorption spectroscopy (MAX-DOAS) measurements in Uccle, Brussels. *Atmos. Meas. Tech.* **2020**, *13*, 5165–5191. [CrossRef]

Disclaimer/Publisher's Note: The statements, opinions and data contained in all publications are solely those of the individual author(s) and contributor(s) and not of MDPI and/or the editor(s). MDPI and/or the editor(s) disclaim responsibility for any injury to people or property resulting from any ideas, methods, instructions or products referred to in the content.